ADVANCED MATERIALS INTERFACES
Open Access
www.advmatinterfaces.de

The Criterion of the Cassie–Baxter and Wenzel Wetting Modes and the Effect of Elastic Substrates on It

*Il Woong Park, Jonas M. Ribe, Maria Fernandino, and Carlos A. Dorao**

Controlling the wettability using microstructures has been studied because of many applications. In particular, bio-mimetic microstructures modeled after the self-cleaning properties of the lotus leaf have been extensively studied. Despite many studies successfully achieving the fabrication of superhydrophobic to superhydrophilic surfaces through the manipulation of microstructures, the effect of rough surfaces on contact angle remains an area of inquiry. In this study, conical microstructures with well-defined geometric parameters are fabricated over a silicon wafer. They are replicated into soft matter that has transparent and flexible characteristics. From the measurement of the contact angle for fabricated surfaces, the prediction of the criteria for transitioning from the Cassie-Baxter state to the Wenzel state can be suggested. Furthermore, the fabrication of an inexpensive, transparent, elastic, and superhydrophobic surface based on truncated micro-conical structures in PDMS can be suggested.

1. Introduction

Controlling the wettability of a surface has been a topic of significant interest due to its numerous practical applications in various fields such as biotechnology, medicine, and heat transfer.[1–7] For example, superhydrophobic surfaces which can be defined by greater than 150° of apparent contact angle have been considered for antifogging,[8–9] anticorrosion,[10–11] antifouling,[12] anti-icing,[13–14] drag reduction,[15] antibacterial,[16–17] energy harvesting[18–19] and condensation.[20–21] Especially, the lotus effect has been extensively studied for the self-cleaning[22–29] which is characterized by a high apparent contact angle and a low contact angle hysteresis or a tilting angle. Several research groups have attempted to mimic these properties by creating artificial self-cleaning surfaces.[22–27] Feng et al. achieved a high apparent contact angle (166°) and a low tilting angle (≈3°) by fabricating aligned carbon nanotubes.[22] Liu et al. showed that the surface becomes super repellent against the liquid in low surface tension by texturing the doubly reentrant structure.[28]

Despite the achievement of fabrication for the surface with the desired wettability, there is still a question about how the rough surface affects the contact angle. There is a well-known diagram which is called the Kao diagram, about the relation about how the rough surface affects contact angle compared with the flat surface with the same substance.[30] It was reported that hydrophilic state can be more hydrophilic and hydrophobic state can be more hydrophobic in rough surfaces. However, it was reported that the hydrophilic surface in the flat surface can be superhydrophilic if the surface is rough enough with three tiers of structures.[25] It has been observed that the number of the tiers of roughness can determine the wettability by Frankiewicz et al. It seems like that there is still open space to understand how the contact angle can be controlled by the roughness of the surface. About the challenges, they were suggested in terms of the optimization of the artificially textured surface for controlling and understanding the wettability.[31]

First focus of this study is understanding how the wettability can be controlled by microstructures across the Cassie-Wenzel transition. As an attempt to understand the effect of the roughness of the surface on the contact angle, quantitative approaches with controlled geometrical parameters and simple structures could be valuable. By us and others, microstructured surfaces with well-defined parameters have been studied.[24–25,28] In particular, we have shown that the apparent contact angle and contact angle hysteresis are directly dependent on the height and center-to-center distance for the conical microstructures.[24] Recently, Wang et al. reported that the theoretical model can predict the apparent contact angle of superhydrophobic surfaces consisting microstructures armour and nanostructures.[1] However, it would be important to advance not only the model for predicting apparent contact angle in the Cassie–Baxter state or Wenzel state, but also the condition for the Cassie-Wenzel transition. The model for the Cassie-Wenzel transition was suggested based on the solid roughness and the contact line

I. W. Park, J. M. Ribe, M. Fernandino, C. A. Dorao
Department of Energy and Process Engineering
Norwegian University of Science and Technology
Trondheim NO-7491, Norway
E-mail: carlos.dorao@ntnu.no
I. W. Park
Department of Mechanical Engineering
Inha University
Incheon 22212, Republic of Korea

The ORCID identification number(s) for the author(s) of this article can be found under https://doi.org/10.1002/admi.202202439.

DOI: 10.1002/admi.202202439

density criterion in the previous studies.[32–34] However, there are only limited studies to evaluate or validate the model for the transition.

Second focus of this study is to suggest inexpensive multipurposed superhydrophobic surface. A relatively simple and inexpensive method for obtaining superhydrophobic surfaces consists of applying a hydrophobic coating to the target substrate. For example, silanization treatments have been used for controlling the wettability.[35–36] Fadeev and McCarthy observed that a planar silicon wafer will be hydrophobic (≈110° of apparent contact angle) after octadecyltrichlorosilane self-assembled monolayer coating.[37] Zimmermann et al. reported that the apparent contact angle increased to 165° with the same silane coating when the silicon was structured with nanofilaments.[36] Silanization has also been applied to bioinspired surfaces for obtaining superhydrophobicity in previous studies.[22–23] However, there is a limitation of the apparent contact angle. An apparent contact angle higher than 150° has not been observed when the silanization process is applied to a smooth surface.[35–36] On the other hand, Chen et al. reported that the cone-like structures can present a robust and easy-repairable superhydrophobic surface by thermal spraying.[37] It was reported that the structures can be fabricated by plasma spray deposition using titania on the shielding plate of stainless-steel mesh. In the following step, composites of polytetrafluoroethylene and nano-copper were deposited by flame spray over the titania coating. 153° of the apparent contact angle and 2° of the sliding angle were reported. However, thermal spray coating can be limited by the operating temperature if the substrate is not applicable to such a severe condition.

To overcome the drawbacks of the microtextured surface and coating for the superhydrophobicity, polydimethylsiloxane (PDMS) could be one of the solutions for a simple fabrication for the superhydrophobic surface. PDMS replication has been well studied in applications such as superhydrophobic surface, lab-on-a-chip, and electronics.[38–40] Considering the replication process, it could be beneficial if the structures can be easily peeled after the molding process. There are also advantages to PDMS itself. They are relatively cheap, replicable, transparent, and bendable. Since they are cheap to replicate it could be beneficial for coating relatively large areas. When considering the transmission properties of the PDMS in the infrared, it could be beneficial to apply for the PV cell. A bendable characteristic could give flexibility to the target surfaces. Furthermore, PDMS replication has been considered for fabricating textured surfaces to obtain an antifouling property[41] and an anti-reflection property.[42] The cone shape could be a proper feature due to its structural stability against the pulling force. In this work, the replicating of the conical microstructure on silicon[24] on PDMS is shown as an alternative to transferring the self-cleaning property. This simple structure can be beneficial because the fabrication of complex structures will be relatively expensive due to the inherent complexity of the process limiting the potential for industrial applications.

In this study, we had a chance to measure the apparent contact angle in each sample of the replication process which are microstructures which are micro cones in silicon, plasma-cleaned micro cones, silanized micro cones, and replicated micro cones into soft material. They have different equilibrium wetting angle and the same geometric parameters. Especially, one of the samples has an elastic characteristic of soft material. Apparent contact angle from zero to 170 degrees is observed by varying the geometric parameters and the surface conditions. From that, we could discuss the concept of the criterion of the Cassie–Baxter and Wenzel wetting modes from the previous study.[32,43–44]

2. Experimental Section

2.1. Fabrication Procedure of Conical Microstructures

The fabrication process is described in **Figure 1** and the dimensions of the microstructures are described in the Supporting

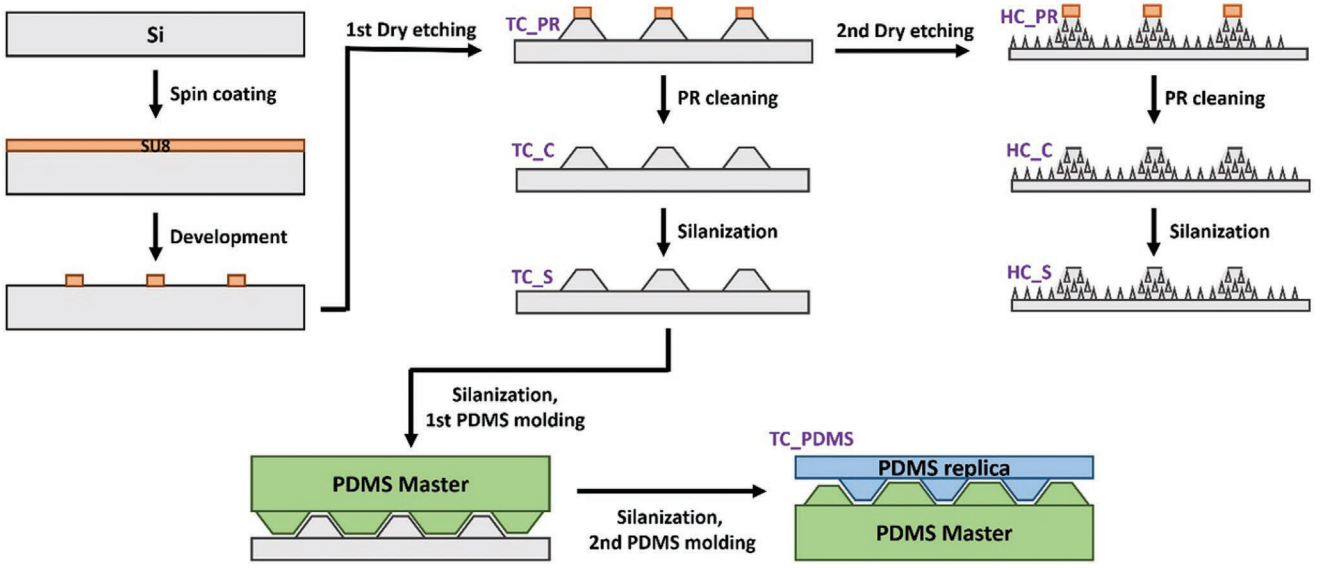

Figure 1. Fabrication process.

Information. The process was conducted on a single-side polished Si wafer ({100}, P-type, containing boron as dopant). The sample TC_ PDMS and HC_P were prepared from the previous study.[10] The process for fabricating the sample of TC_ PDMS and HC_P is described in a previous study.[10] The photoresist (SU-8) layer covering the conical microstructures was removed in an oxygen plasma etching process using an ICP-RIE Cryo Reactor (Plasmalab 100 – ICP180, Oxford Instruments). Energy Dispersive Spectroscopy (EDS) was performed in an FEI Helios dual-beam Focused Ion Beam Scanning Electron Microscopes (FIB-SEM). For the samples TC_C and HC_C, the energy dispersive X-ray spectroscopy did not detect carbon. After removing the photoresist, TC_S and HC_S were silanized in a desiccator using a droplet of Trichloro (1H, 1H, 2H, 2H-perfluorooctyl) silane.

The silicon wafer pattern was replicated in polydimethylsiloxane (PDMS) in a two-step process. First, a replica (dimples) was made from the original Si wafer in PDMS with relatively high stiffness. Second, this PDMS replica was used as a master for molding the original cone structures. Therefore, it was referred to the first replica with dimples as the PDMS master and the second with cones as the PDMS replica.

For the PDMS master, PDMS base and curing agent (Sylgard 184, Dow Corning) were mixed with a weight ratio of 10:1. The mixture was degassed to remove bubbles and cured over the Si master at 65° C for 2 h. The PDMS was peeled from the Si wafer and excess PDMS was cut away using a scalpel. The PDMS master was mounted on a glass slide (75 × 50 mm, Sigma) by treating the backside of the PDMS with a short oxygen plasma and bonding it to the glass. Finally, the PDMS feature side was activated using a short oxygen plasma treatment and silanized in a desiccator using a droplet of Trichloro (1H, 1H, 2H, 2H-perfluorooctyl) silane, similar to the Si wafer. It should be noted that Trichloro is not needed for the further replication process once the PDMS master is coated.

For the PDMS replicas, PDMS base and curing agent (Sylgard 184, Dow Corning) were mixed with the normal weight ratio 10:1. The mixture was degassed to remove bubbles and poured on top of the PDMS master. A glass slide (75 × 50 mm, Sigma) was placed on top of the uncured PDMS and the whole stack was placed in the oven at 65° C for 2 h. The PDMS replica was peeled manually from the PDMS master using the glass slides.

2.2. Scanning Electron Microscopes (SEM)

For the SEM image, an FEI Helios dual-beam Focused Ion Beam Scanning Electron Microscopes (FIB-SEM) was used. The stage was tilted 52° for measuring the height of the microstructures. For the TC_ PDMS, a 10 nm gold layer was deposited by evaporation (Custom ATC-2200 V, AJA International Inc.) before taking SEM images.

2.3. Contact Angle Measurement

The apparent contact angle was measured for every sample. 9.8 µL of distilled water was gently deposited on top of each sample. Advancing and receding contact angles were measured by varying the volume of the droplet between 5 µL and 50 µL. The receding contact angle was measured just before the detachment of the droplet in case of the superhydrophobic condition. The tilting angle was measured by changing the tilted angle of the stage (GNL10/M, Thorlabs). 9.8 µL of a distilled water droplet was deposited before changing the tilted angle of the stage.

3. Results

3.1. Control of Wettability by Micro Conical Structures

Figure 2 shows SEM images of the fabricated samples. Truncated cones with photoresist (TC_PR) and hierarchical cones with photoresist (HC_PR) were fabricated by combined photolithography and dry etching process.[24] TC_PR and HC_PR samples were treated with oxygen plasma to remove the photoresist. After stripping the photoresist, the samples are named cleaned truncated cones (TC_C) and cleaned hierarchical cones (HC_C). The cleaned samples are functionalized with a monolayer of silane and named silanized truncated cones (TC_S) and silanized hierarchical cones (HC_S). TC_S was replicated into PDMS and named truncated cones in PDMS (TC_PDMS). The cleaned hierarchical cones were not replicated into the PDMS due to the fragility of the high aspect ratio structures. The fabrication is described in detail in the methods section.

Figure 3a presents the relation between the apparent contact angle on a textured surface θ^* and the equilibrium wetting angle for the smooth surface of a given material θ_E. For the x-axis, four equilibrium wetting angles which are silicon after

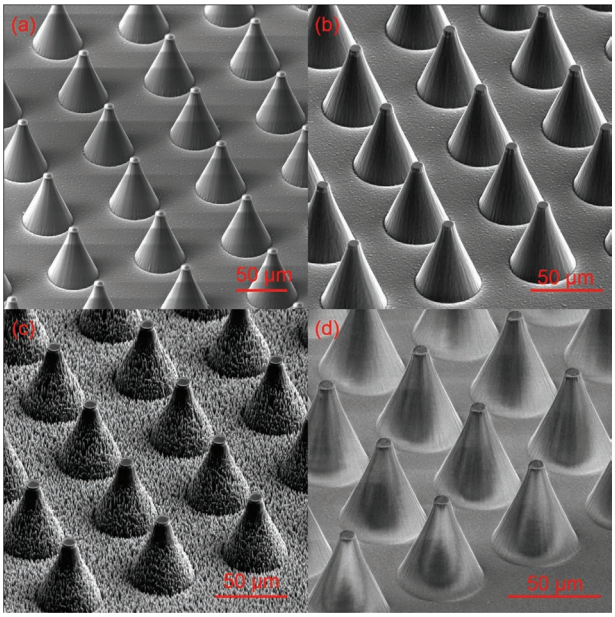

Figure 2. SEM images of micro conical structures. a) Truncated cones with photoresist, TC_PR b) Cleaned truncated cones, TC_C c) Cleaned hierarchical cones, HC_C d) Truncated cones replicated into PDMS, TC_PDMS. TC_PR, TC_C, and TC_PDMS have similar topography and have different equilibrium contact angle.

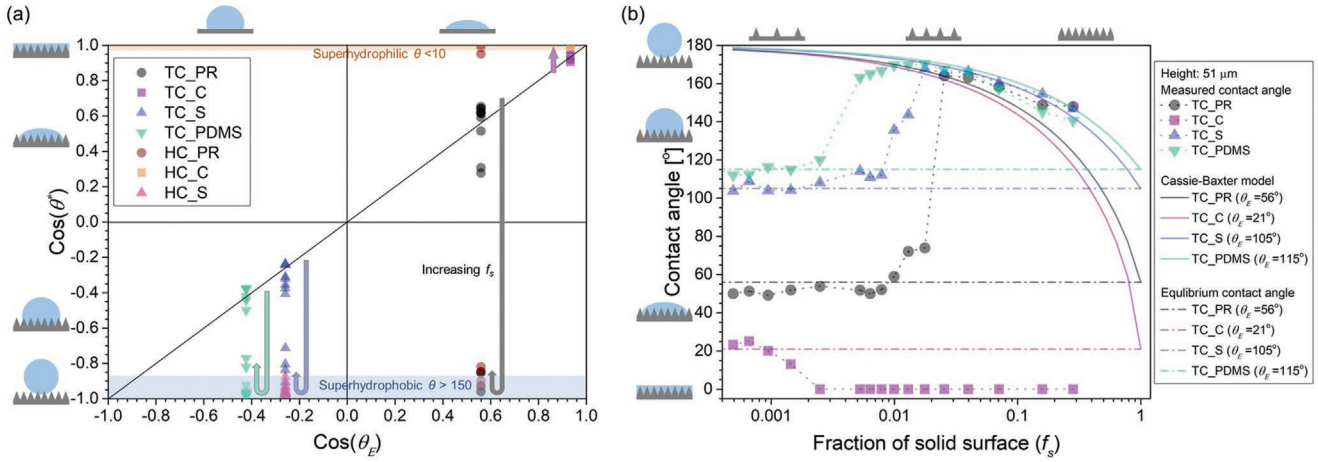

Figure 3. Control of wettability by conical microstructures from superhydrophobic state to superhydrohpilic state. a) Measured apparent contact angle θ^* and the equilibrium wetting angle θ_E for conical microstructures and b) measured apparent contact angle plotted over the Cassie–Baxter model. The superhydrophobic and superhydrophilic states can be achieved by single-tier depends on the geometrical parameters of topography and the equilibrium contact angle.

oxygen plasma treatment (21°), the photoresist (56°), silanized silicon (105°), and PDMS (115°) are considered. The fraction of solid surface (f_s) was defined as the ratio between the area of the top surfaces of microstructures and the total projected area. It is also described in the Supporting Information. Each point represents 16 different fraction of solid surface which are obtained by varying the center-to-center distance between truncated cones which are varying from 15 to 360 micrometers. For each substance, apparent contact angles for the textured surfaces are measured and depicted on the *y*-axis.

Results show that the superhydrophobic state can be obtained with only single-tier topography without double-tier topography. Details of the apparent contact angle for the TC_PR and HC_PR was reported in our previous study.[24] The samples which are hydrophilic in the equilibrium wetting angle as TC_PR and HC_PR can be in a superhydrophobic state. It shows that the superhydrophobic state can be achieved by optimizing the geometrical parameters of single-tier topography without hierarchical structures. However, surfaces become more hydrophilic even though single and double-tier topography were applied, when the equilibrium wetting angle is close to the superhydrophilic state in cases of TC_C and HC_C. It seems like that the apparent contact angle can be varied by the geometric parameter of the single-tier topography but there is the threshold which is the equilibrium wetting angle for achieving superhydrophobic or superhydrophilic states. In the following figures, how the geometric parameters or solid fraction play major roles to determine the apparent contact angle of the roughened surface while the equilibrium wetting angle plays as the thresholds in the Cassie–Baxter state.

Figure 3b shows the apparent contact angle for the TC_PR, TC_C, TC_S, and TC_PDMS over the Cassie–Baxter model. When the fraction of solid surface becomes low, the apparent contact angle is no longer dependent on the fraction of solid surface. In this region, the apparent contact angle is increased by ≈50° when the sample is silanized compared with the case with photoresist. The apparent contact angle increases by another ≈10° when the sample is replicated into PDMS. This could imply that the apparent contact angle is determined by the equilibrium wetting angle which can be applied for the bottom surface between the microstructures when the fraction of solid surface is low.

For conical microstructures with high fraction of solid surface, the apparent contact angle for TC_C is zero while the other three samples have a high apparent contact angle. After the cleaning process, the apparent contact angle of the top surface of the conical microstructure becomes close to that of the polished side of the silicon wafer which gives an apparent contact angle ≈20°. A zero-contact angle for TC_C implies that there is the threshold of equilibrium wetting angle for achieving a superhydrophobic state. This can be understood that the equilibrium wetting angle of the top surface is an important parameter even when the geometric parameter of topography is optimized.

However, a high apparent contact angle is observed for the samples TC_PR, TC_S, and TC_ PDMS with a high fraction of solid surface. It can be discussed by considering the Cassie-Baxter model in solid lines. For the Cassie-Baxter state, the Cassie-Baxter model can be considered to predict the apparent contact angle when the droplet is on top of the structures containing trapped air in the pores between the solid surfaces.[4] In this model, the apparent contact angle can be represented in terms of the equilibrium wetting angle and the solid fraction as:

$$\cos\theta^* = -1 + f_s(\cos\theta_E + 1) \quad (1)$$

where θ^* is the apparent contact angle for the Cassie–Baxter model, f_s is the solid fraction, and θ_E is the equilibrium wetting angle. It shows that superhydrophobic properties of the silicon master are transferred to PDMS in the replication process when comparing them for the high fraction of the solid. Equilibrium wetting angels for corresponding materials are considered for drawing reference lines for the Cassie–Baxter model. It can be observed that experimental results are not following the lines for different equilibrium wetting angles, even

though they have different equilibrium wetting angles. This can disapprove of the hypothesis of the Cassie-Baxter state, which is the area-weighted average of the cosine of the equilibrium wetting angle for the given cases. On the other hand, the solid fraction seems like the main parameter for deciding the apparent contact angle for the Cassie–Baxter state. It should be mentioned that the limitation of the model such as the shape of the structures, the volume of the droplet, and external forces have been already reported in previous studies.[6] Experimental data for hierarchical conical microstructures is reported in the Supporting Information.

3.2. Contact Angle Hysteresis and Tilting Angle

Figure 4a presents the contact angle hysteresis for the TC_ PR, TC_S, and TC_ PDMS. The contact angle hysteresis was obtained by substituting the advancing and receding contact angles in Figure 4b. The contact angle hysteresis is increased with increasing fraction of solid surface for the three samples (TC_PR, TC_S, and TC_ PDMS). After increasing, the contact angle hysteresis suddenly decreases with increasing fraction of solid surface. Therefore, it is possible to consider that there are optimal geometric parameters for obtaining the self-cleaning surface which requires a high apparent contact angle with a low contact angle hysteresis.

Figure 5 shows the tilting angle for TC_S and TC_ PDMS. The two samples presented tilting angles below 5° when adjusting the fraction of the solid surface. For TC_ PDMS, a tilting angle lower than 2 degrees was observed. This minimum tilting angle is lower than for the other samples. It can be understood that the tilting angle can be reduced by decreasing the fraction of solid surface until the high apparent contact angle can be obtained.

The findings of the studies on the Cassie–Baxter state, Cassie–Wenzel transition, and Wenzel state can be summarized as follows:

For the Cassie-Baxter state, the wettability can be dominantly determined by the fraction of the solid surface, while the equilibrium wetting angle could be considered as a threshold. For the Wenzel state, the wettability is determined based on the equilibrium wetting angle, while the surface topography plays no significant role. The Cassie-Wenzel transition can be predicted by considering the criterion for the transition based on the solid-liquid interface roughness.

To obtain the surface with high apparent contact angle with low tilting angle, the fraction of solid surface could be adjusted. For the high apparent contact angle large fraction of solid surface is needed to obtain the Cassie-Baxter state. However, as low as possible fraction of solid surface is required to achieve low tilting angle and low contact angle hysteresis when the Cassie–Baxter state is sustained while the fraction of solid surface is decreased.

For the application, the self-cleaning property is given by a high apparent contact angle, low contact angle hysteresis, and low tilting angle. A structured silicon surface expressing these properties can be replicated in PDMS using soft lithography and obtain similar self-cleaning properties. For the conical microstructures discussed here, the PDMS surface presents a broader range of fraction of solid surface where the self-cleaning property is obtained when compared with the silicon surface it was replicated from.

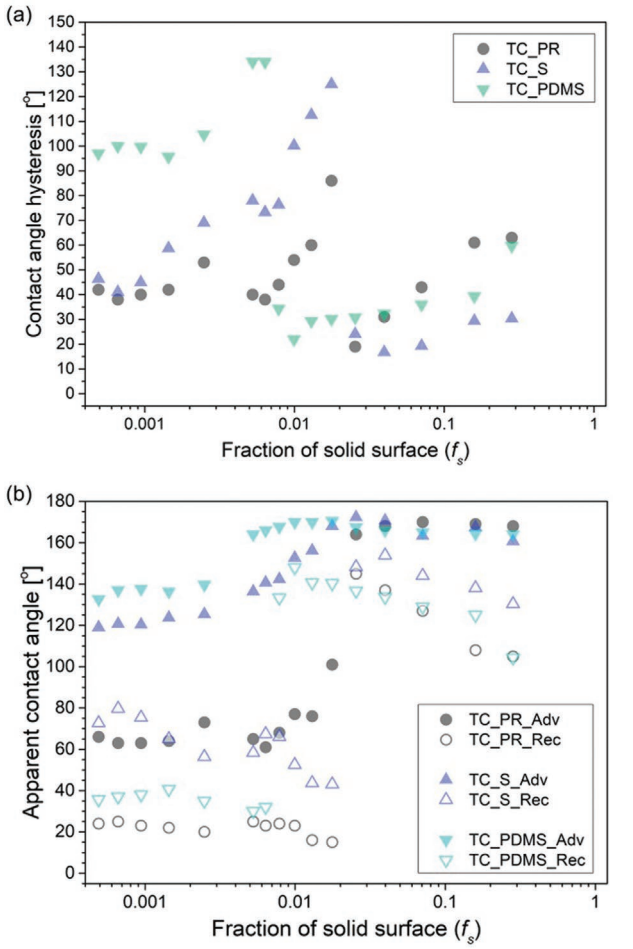

Figure 4. Dynamic contact angle. a) Contact angle hysteresis and b) advancing and receding contact angles of samples.

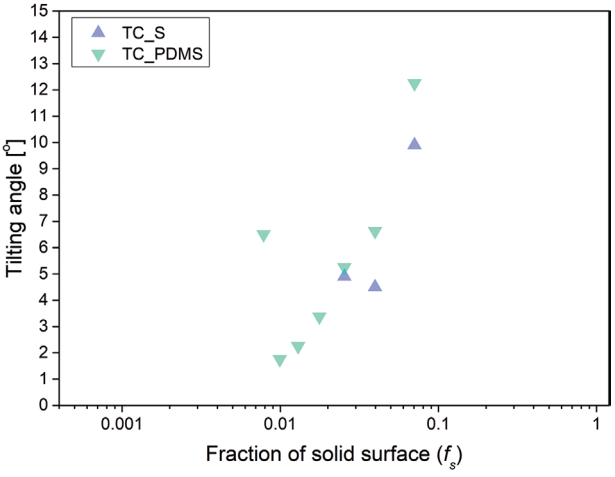

Figure 5. Tilting angle of samples. The PDMS sample shows a broad range of low tilting angle compared to the silanized sample.

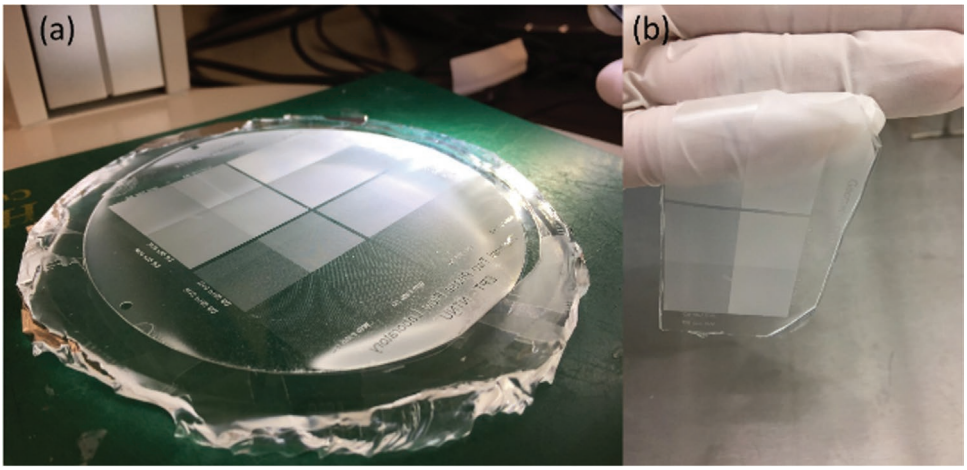

Figure 6. a) PDMS master (4 inches mask), b) TC_PDMS.

The conical microstructures in single-tier were replicated as shown in **Figure 6**. It has an advantage in the peeling process for PDMS replication. This is because the conical shape has structural stability against the pooling force and the microstructure in the single-tier has a smaller interfacial area which causes the pooling force compared with hierarchical structures. From this optimized shape regarding the replication process, it seems possible to obtain a superhydrophobic surface at a low cost. This is because it can be obtained using only the mixture of PDMS base and PDMS curing agent if the PDMS master is prepared once.

4. Discussion

Figure 7 presents the apparent contact angle for three different heights of microstructures and the criterion of the Cassie-Wenzel transition. The criterion of the Cassie-Wenzel transition can be written as $\cos\theta_{cr} = (f_s - 1)/(r - f_s)$, where f_s is the fraction of the solid surface and r is the solid-liquid interface roughness.[32] Details of the fraction of the solid surface and the solid-liquid interface roughness are reported in the Supporting Information.

Wetting transitions corresponding to the breakdown of the superhydrophobic state is observed at the cross-section between the criterion for 0.8 of penetration ratio and equilibrium contact angle as depicted as arrows except for the sample in PDMS. It was a noteworthy observation that the geometric conditions for wetting transition, characterized by the breakdown of the superhydrophobic state, can be predicted by taking into account the 0.8 penetration ratio and equilibrium contact angle for conical microstructures. This discovery has important implications for understanding and controlling the wetting properties of surfaces.

Even though the drastic Cassie–Wenzel transition was observed in silicon, a sudden change in the apparent contact angle was not observed in PDMS. The difference between the profile of the apparent contact angle could be oriented from the elasticity of soft material. For the PDMS sample, the cross-section between the criterion and equilibrium contact angle didn't point out the location of the Cassie–Wenzel transition in Figure 7b. This could be attributed to the elastic characteristic of the PDMS as soft material. The deformation of the elastic substrate can be considered as the increase of the equilibrium contact angle as shown in **Figure 8**. The deformation of the soft material was observed in the previous study.[45]

The contact angle relative to the horizon at the pinning of the micropillar can be considered as the summation of the advancing contact angle for the smooth surface and the 90° as shown in Figure 8b. For that, we should assume that the liquid-solid interface is pinned at the sidewall of the micropillar. When we consider the conical structures the contact angle relative to the horizon will be decreased by the half apex angle of the conical structure as depicted in Figure 8c. The criterion of the Cassie-Wenzel transition was calculated by considering the liquid-solid interface in this figure. It means that the deformation of the soft material was not considered in the calculation. However, it seems that the deformation of the soft material could increase the contact angle relative to the horizon as described in Figure 8d. It could be the reason why the Cassie–Wenzel transition is located in a lower fraction of solid surface because the additional contact angle for the equilibrium contact angle could shift the cross-section between the criterion of the Cassie–Wenzel transition and the adjusted equilibrium contact angle.

In Figure 7, the Cassie-Wenzel transition occurs for 31, 51, and 71 μm of height when the θ_E is 105°. However, the Cassie-Baxter state wasn't observed when the θ_E is 21°. The possible explanation of the failure of forming a droplet on the microstructures in the Cassie-Baxter state can be explained as presented in Figure 8e. As we discussed above, the contact angle relative to the horizontal can be drawn for the low equilibrium contact angle. When we consider the low equilibrium contact angle, the liquid-gas contact lines from the pinned point in both microstructures couldn't be connected because of the low contact angle relative to the horizon. It shows that the criteria to achieve the Cassie–Baxter state could be the combination of the advancing equilibrium contact angle and the half apex angle of the microstructures. In the case of 56° of θ_E, the Cassie-Baxter state can't be achieved for 31 μm of height. It could be understood that the liquid-gas interface lines from the pinned point

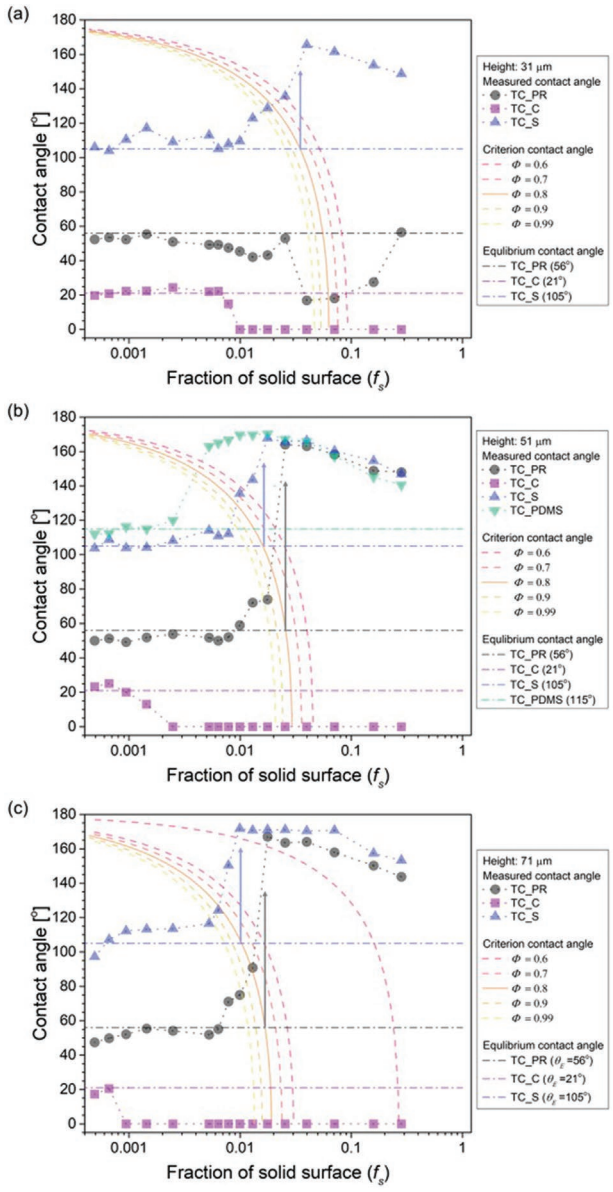

Figure 7. The criterion of the Cassie–Wenzel transition. Measured apparent contact angles are depicted for a) 31, b) 51, and c) 71 μm of heights of microstructures. Dashed lines present the criterion of the Cassie-Wenzel transition for varying penetration ratio and solid line present that for 0.8 of penetration ratio. Dash-dotted lines represent the equilibrium contact angle. The criterion implies that the droplet forms the Cassie-Baxter state when the criterion is lower than the equilibrium contact angle. The cross-section between them can be considered the point of the Cassie–Wenzel transition.

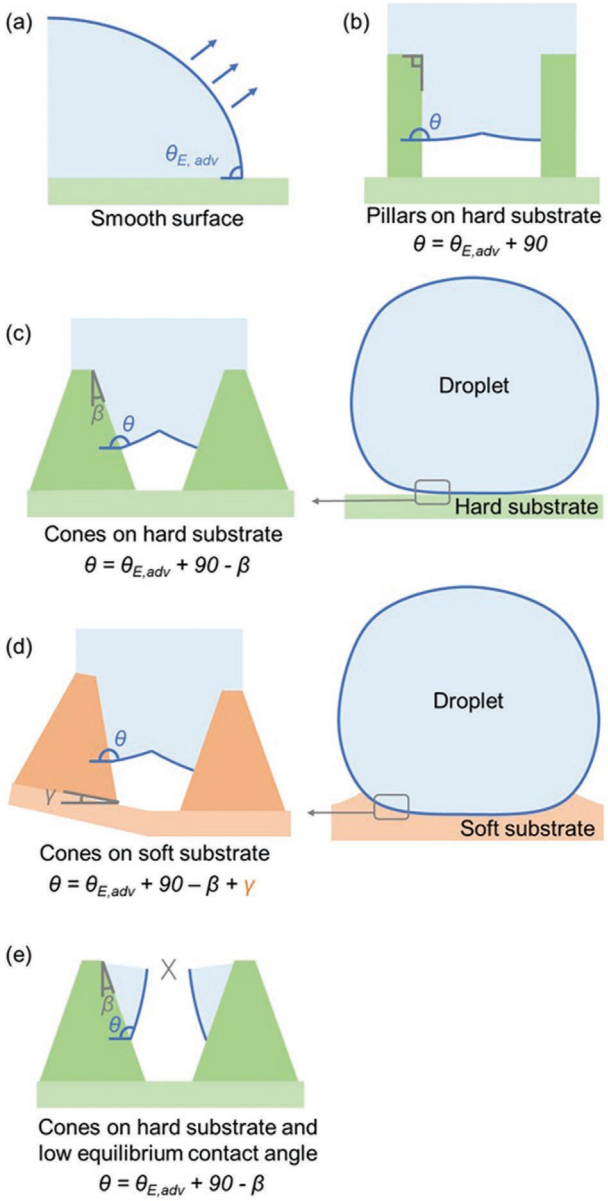

Figure 8. Schematic diagram of the contact angle relative to the horizon in a) smooth surface, b) micro pillars, c) micro cones on hard substrate, d) micro cones on soft substrate, and e) the failure of forming droplet on structure. We compared the contact angle relative to the horizon θ to evaluate the wettability of the surface with microstructures. It is assumed that the liquid-solid interface is pinned at the certain height of microstructure and the advanced contact angle for the smooth surface is considered for deriving the contact angle relative to the horizon. The contact angle relative to the horizon is affected by the half apex angle of conical structures β and the deformation angle of soft material γ.

in both microstructures could be connected when the structures are high even though the equilibrium contact angle is low.

5. Conclusion

In this study, conical microstructures with well-defined geometric parameters were fabricated on silicon, cleaned by plasma, silanized, and replicated into the soft substrate in sequence. The wettability of the conical microstructures was examined in each process. we were able to obtain a range of apparent contact angles for varying geometric parameters, and for four different equilibrium contact angles. The study determined the geometric parameters of micro conical structures that exhibit super-hydrophilic and super-hydrophobic properties. Moreover, our observations revealed that the Cassie-Wenzel

transition occurred at different fractions of the solid surface depending on the equilibrium contact angle and the geometric parameters. The significant discovery in this study was that the Cassie-Wenzel transition was located where the criterion of the Cassie-Wenzel transition for 0.8 penetration ratio for conical structures in silicon substrate. Furthermore, we discussed the shift of the Cassie-Wenzel transition in soft substrate based on the measured apparent contact angle. Furthermore, from the optimization of the solid fraction which is critical for single-tier structures, it could be able to open the possibility for the application based on the replication. As PDMS is a relatively inexpensive material and soft lithography allows for multiple replications, this represents an important step towards low-cost self-cleaning surfaces. Furthermore, the transparency and elasticity of PDMS open up the possibility for novel applications. This study not only provides insight into the wetting transition, but also has the potential to lead to practical applications in various fields.

Supporting Information

Supporting Information is available from the Wiley Online Library or from the author.

Acknowledgements

The Ph.D. fellowship (Il-Woong Park) financed by the NTNU-SINTEF Gas Technology Centre is gratefully acknowledged. The Research Council of Norway is acknowledged for the support to the Norwegian Micro- and Nano-Fabrication Facility, NorFab, project number 295864. This work was supported by the National Research Foundation of Korea (NRF) grant funded by the Korean government(MSIT) (No. RS-2022-00144494).

Conflict of Interest

The authors declare no conflict of interest.

Author Contributions

I.W.P. suggested the initial concept, fabricated samples, and measured contact angle. J. M. R. performed PDMS replication. M. F. and C. A. D. supervised the work. I. W. P., J. M. R., M. F., and C. A. D. wrote the manuscript.

Data Availability Statement

The data that support the findings of this study are available in the Suppporting Information of this article.

Keywords

bio-mimetic microstructures, superhydrophobic, super hydrophilic, self-cleaning characteristics, wettability

Received: December 6, 2022
Revised: February 7, 2023
Published online: March 22, 2023

[1] D. , Q. Sun, M. J. Hokkanen, C. Zhang, F.-Y. Lin, Q. Liu, S.-P. Zhu, T. Zhou, Q. Chang, B. He, Q. Zhou, L. Chen, Z. Wang, R. H. A. Ras, X. Deng, *Nature* **2020**, *582*, 55.
[2] P. Lv, Y. Xue, Y. Shi, H. Lin, H. Duan, *Phys. Rev. Lett.* **2014**, *112*, 196101.
[3] D. Li, Y. Xue, P. Lv, S. Huang, H. Lin, H. Duan, *Soft Matter* **2016**, *12*, 4257.
[4] A. B. D. Cassie, S. Baxter, *Trans. Faraday Soc.* **1944**, *40*, 546.
[5] R. N. Wenzel, *Ind. Eng. Chem.* **1936**, *28*, 988.
[6] E. Bormashenko, *Adv. Colloid Interface Sci.* **2015**, *222*, 92.
[7] E. Bormashenko, *Colloids Surf. A* **2009**, *345*, 163.
[8] T. Mouterde, G. Lehoucq, S. Xavier, A. Checco, C. T. Black, A. Rahman, T. Midavaine, C. Clanet, D. Quéré, *Nat. Mater.* **2017**, *16*, 658.
[9] Z. Sun, T. Liao, K. Liu, L. Jiang, J. H. Kim, S. X. Dou, *Small* **2014**, *10*, 3001.
[10] Z. Wang, Y. Su, Q. Li, Y. Liu, Z. She, F. Chen, L. Li, X. Zhang, P. Zhang, *Mater. Charact.* **2015**, *99*, 200.
[11] T. T. Isimjan, T. Wang, S. Rohani, *Chem. Eng. J.* **2012**, *210*, 182.
[12] J. A. Barish, J. M. Goddard, *Food Bioprod. Process.* **2013**, *91*, 352.
[13] Y. Tang, Q. Zhang, X. Zhan, F. Chen, *Soft Matter* **2015**, *11*, 4540.
[14] N. Wang, D. Xiong, Y. Deng, Y. Shi, K. Wang, *ACS Appl. Mater. Interfaces* **2015**, *7*, 6260.
[15] G. Mchale, M. I. Newton, N. J. Shirtcliffe, *Soft Matter* **2010**, *6*, 714.
[16] M. Wu, B. Ma, T. Pan, S. Chen, J. Sun, *Adv Funct Mater* **2016**, *26*, 569.
[17] G. S. Watson, D. W. Green, L. Schwarzkopf, X. Li, B. W. Cribb, S. Myhra, J. A. Watson, *Acta Biomater.* **2015**, *21*, 109.
[18] D. Choi, S. Lee, S. M. Park, H. Cho, W. Hwang, D. S. Kim, *Nano Res.* **2015**, *8*, 2481.
[19] N. Miljkovic, D. J. Preston, R. Enright, E. N. Wang, *Appl. Phys. Lett.* **2014**, *105*, 013111.
[20] N. Miljkovic, D. J. Preston, R. Enright, E. N. Wang, *ACS Nano* **2013**, *7*, 11043.
[21] D. Yoon, C. Lee, J. Yun, W. Jeon, B. J. Cha, S. Baik, *ACS Nano* **2012**, *6*, 5980.
[22] L. Feng, S. Li, Y. Li, H. Li, L. Zhang, J. Zhai, Y. Song, B. Liu, L. Jiang, D. Zhu, *Adv. Mater.* **2002**, *14*, 1857.
[23] K. Liu, X. Yao, L. Jiang, *Chem. Soc. Rev.* **2010**, *39*, 3240.
[24] I. W. Park, M. Fernandino, C. A. Dorao, *Adv. Mater. Interfaces* **2018**, *5*, 1701039.
[25] C. Frankiewicz, D. Attinger, *Nanoscale* **2016**, *8*, 3982.
[26] W. Zhang, W. Ding, M. Fernandino, C. A. Dorao, *ACS Appl. Nano Mater.* **2019**, *2*, 7696.
[27] W. Ding, M. Fernandino, C. A. Dorao, *Appl. Phys. Lett.* **2019**, *115*, 053703.
[28] T. L. Liu, C.-J. C. Kim, *Science* **2014**, *346*, 1096.
[29] R. Blossey, *Nat. Mater.* **2003**, *2*, 301.
[30] T. Onda, S. Shibuichi, N. Satoh, K. Tsujii, *Langmuir* **1996**, *12*, 2125.
[31] Y. Y. Yan, N. Gao, W. Barthlott, *Adv. Colloid Interface Sci.* **2011**, *169*, 80.
[32] J. Bico, U. Thiele, D. Quéré, *Colloids Surf. A* **2002**, *206*, 41.
[33] C. W. Extrand, *Langmuir* **2004**, *20*, 5013.
[34] H. Sun, W. Tian, Y. Sun, M. Li, *Colloids Surf A Physicochem Eng Asp* **2022**, *638*, 128143.
[35] A. Y. Fadeev, T. J. Mccarthy, *Langmuir* **2000**, *16*, 7268.
[36] J. Zimmermann, M. Rabe, G. R. J. Artus, S. Seeger, *Soft Matter* **2008**, *4*, 450.
[37] X. Chen, Y. Gong, D. Li, H. Li, *Colloids Surf. A* **2016**, *492*, 19.
[38] Q. Cheng, M. Li, Y. Zheng, B. Su, S. Wang, L. Jiang, *Soft Matter* **2011**, *7*, 5948.
[39] G. Comina, A. Suska, D. Filippini, *Lab Chip* **2014**, *14*, 424.
[40] Y. Zhang, Y. Hu, P. Zhu, F. Han, Y. Zhu, R. Sun, C.-P. Wong, *ACS Appl. Mater. Interfaces* **2017**, *9*, 35968.

[41] Z. Chen, W. Zhao, J. Xu, M. Mo, S. Peng, Z. Zeng, X. Wu, Q. Xue, *RSC Adv.* **2015**, *5*, 36874.
[42] J.-H. Shin, K.-S. Han, H. Lee, *Prog. Photovolt: Res. Appl.* **2011**, *19*, 339.
[43] A. J. B. Milne, A. Amirfazli, *Adv Colloid Interface Sci* **2012**, *170*, 48.
[44] J. Bico, C. Marzolin, D. Quéré, *Europhys Lett* **1999**, *47*, 220.
[45] F. Du, J. Huang, H. Duan, C. Xiong, J. Wang, *Sci. Rep.* **2016**, *6*, 25653.